Statistical properties of the heat transport in a model of rotating Bénard convection

M. Neufeld and R. Friedrich
Institut für Theoretische Physik und Synergetik, Universität Stuttgart, Pfaffenwaldring 57/4, D-70550 Stuttgart, Germany
(Received 11 March 1994; revised manuscript received 28 October 1994)

Using a previously devised model equation [Z. Phys. B **92**, 243 (1993)], we study pattern formation in rotating Bénard convection. We focus on the statistical properties of the heat transport in the regime where the roll solutions exhibit a Küppers-Lortz type instability. Due to this instability, spatially disordered patterns emerge. For these patterns we derive a stochastic differential equation for a quantity related to the heat transport. The corresponding stationary probability distribution accurately approximates the one obtained from a numerical evaluation of the model equation.

PACS number(s): 47.27.Te, 47.20.−k, 47.27.Cn

I. INTRODUCTION

One of the most extensively studied systems in the field of pattern formation in nonequilibrium systems is Rayleigh-Bénard thermal convection in a fluid layer heated from below. However, many geophysical and astrophysical convection problems combine thermally induced buoyancy as well as coriolis forces induced by rotation. Therefore Rayleigh-Bénard convection in fluid layers rotating about a vertical axis is a hydrodynamical system of significant importance. Recently, it is under investigation due to the existence of interesting nonvariational aspects of pattern formation as a result of the Küppers-Lortz instability [1]. Above a critical rotation rate, convection rolls lose their stability with respect to rolls inclined at an angle of about 60° in the sense of rotation. The new rolls undergo the same instability, so that there is no stable steady-state pattern. As a result, spatially disordered patterns arise already close to the onset of convection.

The patterns generated by the Küpper-Lortz instability have been theoretically described by Busse and Heikes [2] using amplitude equations for three rolls including an angle of 60°. This model contains an attracting heteroclinic cycle connecting three fixed points corresponding to the three different roll solutions. Recently, Tu and Cross [3] have performed numerical investigations of an extension of these amplitude equations, where a spatial variation of the amplitudes has been introduced. Since the patterns that are found in experiments consist of rolls with more than three different directions, we have focused on a theoretical description using rotational invariant model equations, which are extensions of the Swift-Hohenberg equation [4].

At large rotation rates, one observes disordered patterns consisting of patches of differently orientated convection rolls separately showing the behavior characteristic of the Küppers-Lortz instability [2]. Similar types of patterns can be calculated by the model equation devised in [5]. It is evident that these disordered patterns need a statistical description. The purpose of the present paper is to develop, starting from our model equation (1), a statistical theory for the total heat transport across the layer. The heat transport is usually expressed in terms of the Nusselt number. The Nusselt number is a spatial average. By applying mean-field-type arguments to the evolution equation of a quantity that is directly related to the Nusselt number, we shall derive a nonlinear stochastic differential equation for this quantity. We show that the distribution function obtained from the corresponding Fokker-Planck equation accurately fits the one calculated from the direct numerical evaluation of the model equation. The paper is organized as follows. In Sec. II we specify the model equation, the expression of the Nusselt number, and consider the various instabilities of the family of roll solutions. Then we describe some pattern forming processes in circular geometries. Section III is devoted to an analysis of the heat transport in the Küppers-Lortz unstable regime.

The aim of the present paper is the statistical treatment of pattern generated by the evolution equation (1). Therefore, we do not consider the quantitative comparison between our theoretical results and experiments. Rather, we want to point out that a similar statistical analysis can be applied to experimentally obtained data of the Nusselt number.

II. MODEL EQUATION

Close to instability, pattern formation in a nonequilibrium system can be described by defining a suitable order parameter and deriving the corresponding order parameter equation, which governs its temporal evolution [6,7]. Since the nonlinear terms of this order parameter equation turn out to be rather complicated, a model equation has been devised that contains the main ingredients of the pattern forming process in rotating Bénard convection [5,8,9]:

$$\begin{aligned}\dot{\psi}(\mathbf{x},t)&=\hat{L}(\Delta)\psi(\mathbf{x},t)+2\psi_s(\mathbf{x},t)\Delta\psi(\mathbf{x},t)\\&\quad+\nabla\psi(\mathbf{x},t)\cdot\nabla\psi_s(\mathbf{x},t)\\&\quad+\mathrm{Ta}\beta\mathbf{e}_z\cdot[\nabla\psi(\mathbf{x},t)\times\nabla\psi_s(\mathbf{x},t)]\ ,\\\psi_s(\mathbf{x},t)&=[\nabla\psi(\mathbf{x},t)]^2-\psi(\mathbf{x},t)\Delta\psi(\mathbf{x},t)\ ,\\\hat{L}(\Delta)&=\varepsilon-(1+\Delta)^2\ .\end{aligned}\tag{1}$$

The first control parameter labeled with ε denotes the reduced Rayleigh number $\varepsilon=(R-R_c)/R_c$. The second control parameter Ta is called the Taylor number, which is proportional to the rotation frequency Ω:

$$\mathrm{Ta}=\frac{2\Omega d^2}{\nu} , \tag{2}$$

where d is the thickness of the fluid layer and ν is the kinematic viscosity. The proportionality parameter β depends on the vertical boundary conditions of the system; in the case of stress-free boundary conditions one gets

$$\beta=\frac{1}{\pi^2+k_c^2}\left[1+\frac{6k_c^2(\pi^2+k_c^2)^2}{4\pi^2(\mathrm{Ta})^2+(4\pi^2)^3}\right] , \tag{3}$$

where k_c describes the critical wave number. We refer the reader to [5] for details.

In general, a derivation of the order parameter equation from the basic equations leads to nonlinear terms, which turn out to be nonlocal in space. However, for the purposes of the present paper, it will be sufficient to use Eq. (1), which stems from a suitable approximation of these nonlocal nonlinear interaction terms. Here, as explained in [5], we consider stress-free and ideally heat conductive boundary conditions.

The order parameter $\psi(\mathbf{x},t)$ describes the contribution of the unstable modes to the temperature field in a horizontal plane inside the fluid layer. Using the simplifications leading from the order parameter equation to the model equation [5], the deviation of the temperature field from the linear temperature profile of the purely heat conductive state is given by

$$\Theta(\mathbf{r},t)=\psi(\mathbf{x},t)\sin\left[\frac{\pi z}{d}\right]+\psi_s(\mathbf{x},t)\sin\left[\frac{2\pi z}{d}\right] . \tag{4}$$

The model equation (1) has the following family of roll solutions:

$$\psi_k(\mathbf{x},t)=2A(k)\sin(kx+\varphi_0) ,$$
$$A^2(k^2)=\frac{\epsilon-(1-k^2)^2}{8k^4} . \tag{5}$$

These roll solutions become unstable due to two types of linear instabilities. Long scale instabilities modulate the direction and the wavelength of the rolls on a spatial scale that is large compared to the thickness of the rolls. The other kind of instability is a cross roll instability by which rolls become unstable with respect to differently orientated rolls. The occurrence of the Küpper-Lortz instability in a rotating system with high Prandtl number arises if all roll solutions are unstable with respect to this cross roll instability.

The stability analysis for the roll solutions of the basic hydrodynamic equations and arbitrary Prandtl numbers has been performed by Clever and Busse [10]. For a detailed stability analysis of the model equation (1) we refer the reader to [5]. Figure 1 shows the resulting stability diagrams for different Taylor numbers. The shaded regions denote the existence of stable roll solutions. These regions shrink to zero if the Taylor number is increased above the critical one ($\beta\mathrm{Ta}_c=2\sqrt{2}$).

An experimentally accessible quantity is the total heat transport, which is represented in a dimensionless form by the Nusselt number Nu [11]. This number is defined as the ratio of the total heat flux and the conductive heat flux [12]

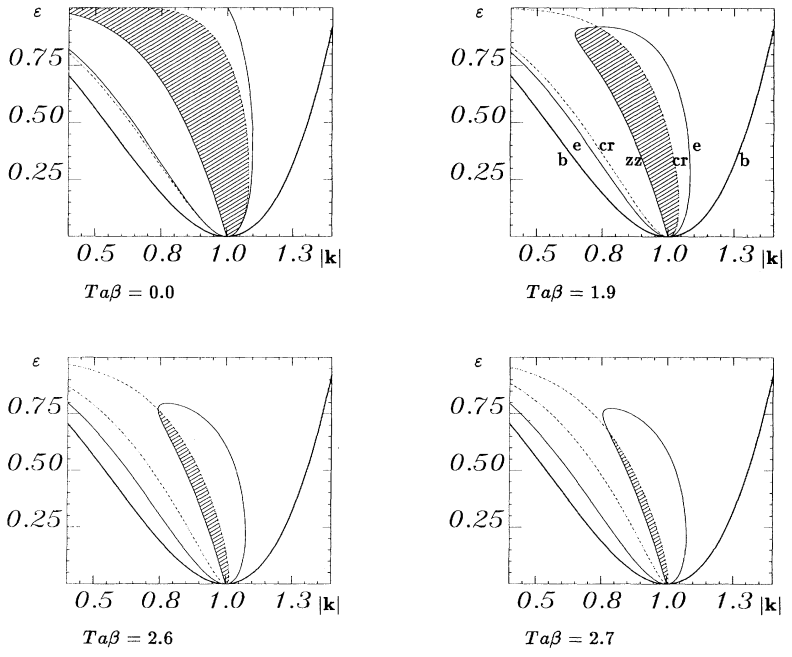

FIG. 1. Stability diagrams of roll solutions of Eq. (1) for various Taylor numbers.

$$\mathrm{Nu}=\frac{(\text{total heat flux in convective regime})}{(\text{heat flux in conductive regime})}=-\frac{\kappa\left\langle\frac{\partial}{\partial_z}T(\mathbf{r},t)\right\rangle_{z=1}}{\kappa\beta} . \tag{6}$$

The brackets $\langle\ \rangle_{z=h}$ denote the mean value in the horizontal plane at $z=h$. The temperature $T(\mathbf{r},t)$ is given by the linear temperature profile of the conductive state and the deviation $\Theta(\mathbf{r},t)$:

$$T(\mathbf{r},t)=T_{z=0}-\beta z+\beta d\Theta(\mathbf{r},t) . \tag{7}$$

Using the above representation of $\Theta(\mathbf{r},t)$ (4) we obtain the following expression for the Nusselt number:

$$\mathrm{Nu}=1-2\pi\frac{\int d\mathbf{x}\,\psi_s(\mathbf{x},t)}{\int d\mathbf{x}} . \tag{8}$$

A straight roll pattern with a wave vector $\mathbf{k}$ has a Nusselt number $\mathrm{Nu}(\mathbf{k})=1+2\pi\mathbf{k}^2|\psi|^2$. The integration of Eq. (1) leads to a time signal of the Nusselt number (8). In the following we shall focus on the dynamical as well as the statistical properties of this number.

III. PATTERN FORMATION IN A CIRCULAR REGION

The present section aims at presenting patterns that can be calculated by the model equation (1) in a circular vessel in order to show that the main characteristics of the experimentally obtained features [11] are contained in the evolution equation (1). Thereby, the following boundary conditions have been used:

$$\psi(\mathbf{x},t)_{\partial V}=d,\quad \mathbf{n}\cdot\nabla\psi(\mathbf{x},t)_{\partial V}=0 . \tag{9}$$

The control parameter d parametrizes heating at the lateral walls; $d=0$ represents a rigid horizontal boundary with vanishing sidewall forcing. In this case, the convective rolls tend to align perpendicularly to the boundary.

For $d=0$ the system already exhibits a complex temporal behavior at small rotation rates below the Küppers-Lortz instability (see Fig. 2). This time dependence is due to defects moving along the circular boundaries. Figure 2 shows a pattern in a container with aspect ratio comparable to an experiment by Zhong, Ecke, and Steinberg [13]. The pattern at $t=180$ is characterized by the existence of three foci. A defect moves in the direction opposite to the externally applied rotation. Figure 3 shows the temporal evolution of the pattern in a higher aspect ratio system. Here, defects located close to the boundary are driven to move in the sense of the externally applied rotation leading to an s-shaped deformation of the straight roll pattern inside the container. On the other hand, defects nucleated at the edge between the defect regions and the bulk pattern of nearly parallel rolls move in the sense opposite to the external rotation. The motion of the defects as well as the bending of the rolls lead to a slight decrease of the average heat transport. When the moving defect is absorbed in the other defect region a sudden increase of the Nusselt number is observed and a similar process starts again. However, the

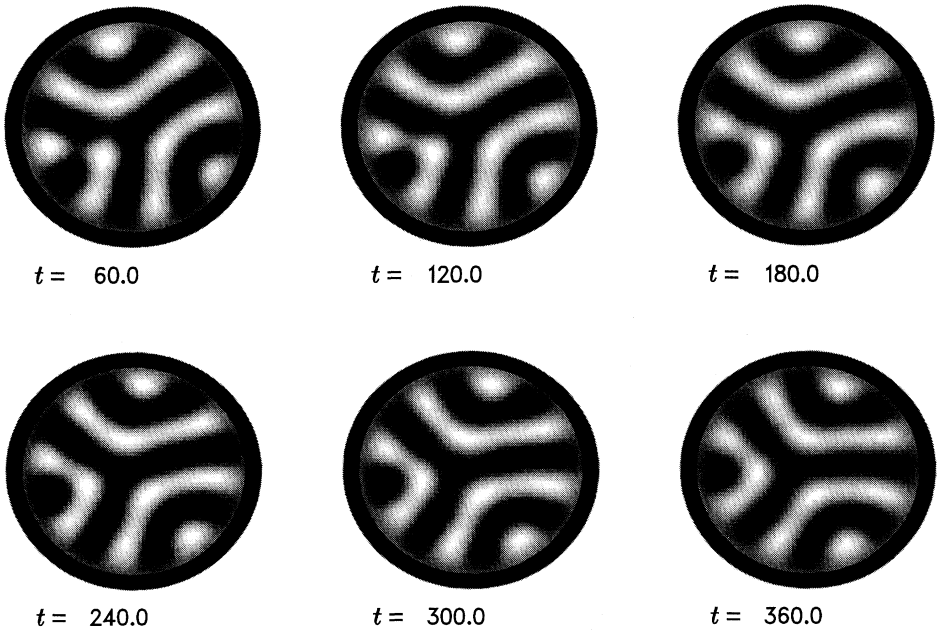

FIG. 2. Temporal evolution of convection patterns in a low aspect ratio system for a small rotation rate. The pattern is formed by three foci that are located at the lateral boundary. The pattern is drifting very slowly.

temporal evolution is not time periodic.

The behavior of the patterns above the Küppers-Lortz instability, i.e., the reorientation of the direction of the convective rolls, is dominated by front propagation. As already mentioned, the defect regions in the circular container induce a bending of the rolls leading to an s-shaped roll pattern. This s-shaped pattern can be viewed as three differently oriented roll patches separated by two domain walls. These domain walls start to move, eventually annihilating each other. A reorientation of the roll orientation has taken place. The bending of the rolls and the motion of the domain walls are connected with a decrease of the Nusselt number where the annihilation of the domain walls lead to a sudden increase of the heat transport. Due to the spatial complexity of the patterns, this process occurs irregularly in time.

A weak sidewall forcing $d \neq 0$ leads to convection rolls aligned parallel to the circular boundary. This can lead to concentric as well as spiral patterns below the critical Taylor number [see Fig. 4(a)]. As an example, we describe the formation of a spiral pattern. Starting from a random pattern, we obtain a structure where rolls are, in some regions, perpendicular or parallel to the lateral wall. At the boundaries between parallel and perpendicular oriented rolls, domain walls form, penetrating nearly to the center of the cell. Two such domain walls have formed in the upper region of the pattern at $t = 11\,000$. These domain walls start to move in opposite directions,

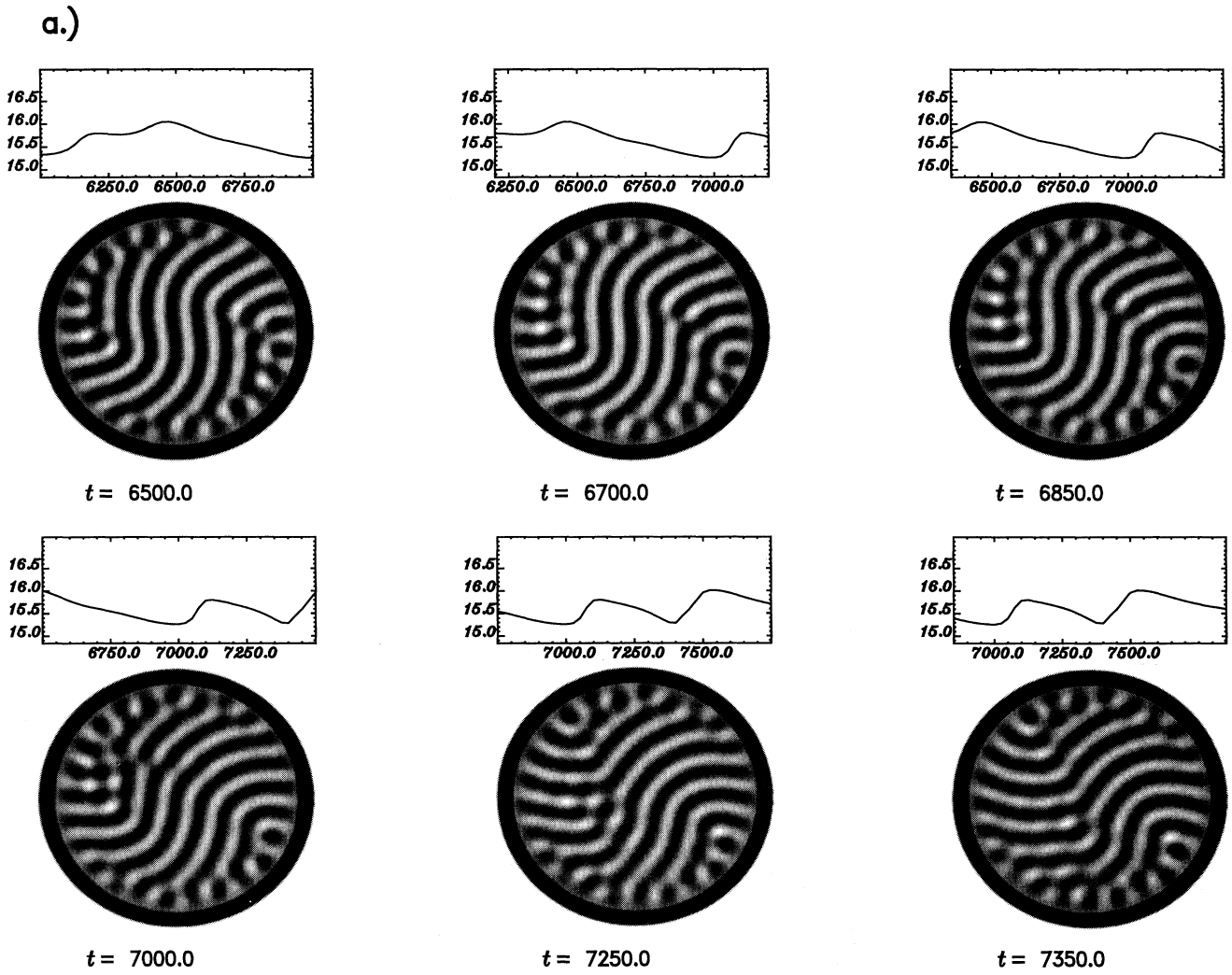

FIG. 3. Temporal evolution of the order parameter field and the Nusselt number in the case of vanishing lateral forcing $d = 0.0$ and $\varepsilon = 0.1$. (a) Defect motion in the case of a Taylor number $\mathrm{Ta} = 2.0 < \mathrm{Ta}_c$. (b) Front propagation in the case of a Taylor number $\mathrm{Ta} = 3.0 > \mathrm{Ta}_c$.

eventually leading to the spiral pattern. This pattern rotates slowly.

For Taylor numbers Ta above the critical one, the spiral is destroyed by Küppers-Lortz instability. However, it is formed again leading to a continuous emergence and destruction of spirals. It would be interesting whether similar spatiotemporal behavior, i.e., a spiral pattern undergoing a Küppers-Lortz transition, can be observed in a suitable experimental setup [see Fig. 4(b)].

IV. KÜPPERS-LORTZ TURBULENCE

By numerical means, we also investigated the order parameter equation (1) for the case of periodic boundary conditions for various values of the control parameter Ta. For high values of the Taylor number, one obtains spatially disordered patterns. The existence of such disordered patterns are well-known from experiments [14]. We have used the model equation to investigate the dynamical as well as the statistical properties of these time dependent disordered patterns, which we shall denote as "Küppers-Lortz turbulence."

For moderate Taylor numbers, the patterns exhibit spatial coherence. However, the reorientation of the rolls does not occur uniformly in space, but appears locally. After the nucleation of a small region of rolls with the new roll orientation, front propagation occurs [see Fig. 5(a)]. As a main characteristic, we note that a region of different roll orientation can be nucleated inside a larger region of relatively uniform convective rolls. In other words, the system is apparently able to spontaneously generate domain walls [see Fig. 5(a)]. For higher values of the Taylor number, the spatial coherence is destroyed leading to irregular patterns [see Fig. 5(b)].

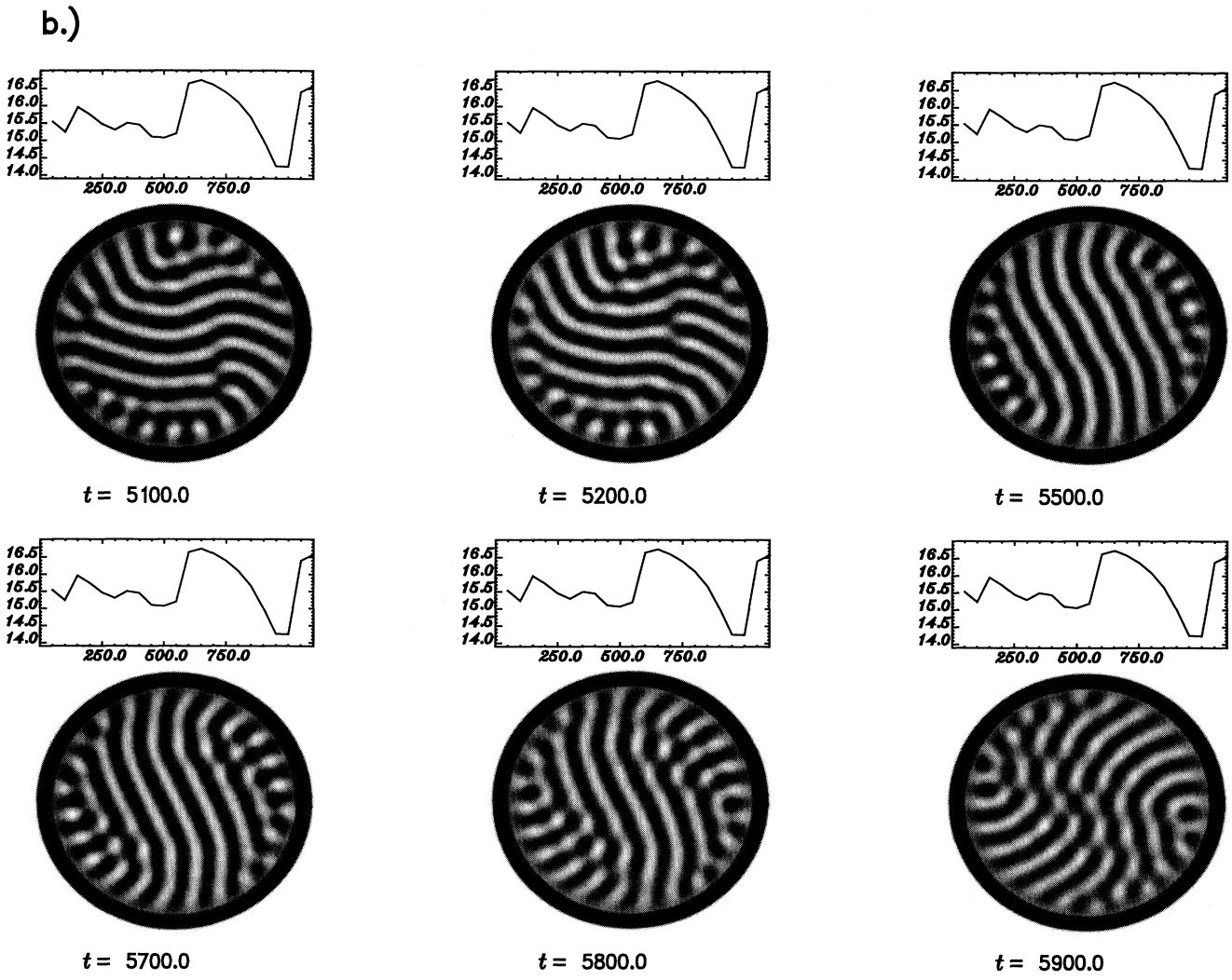

FIG. 3. (*Continued*).

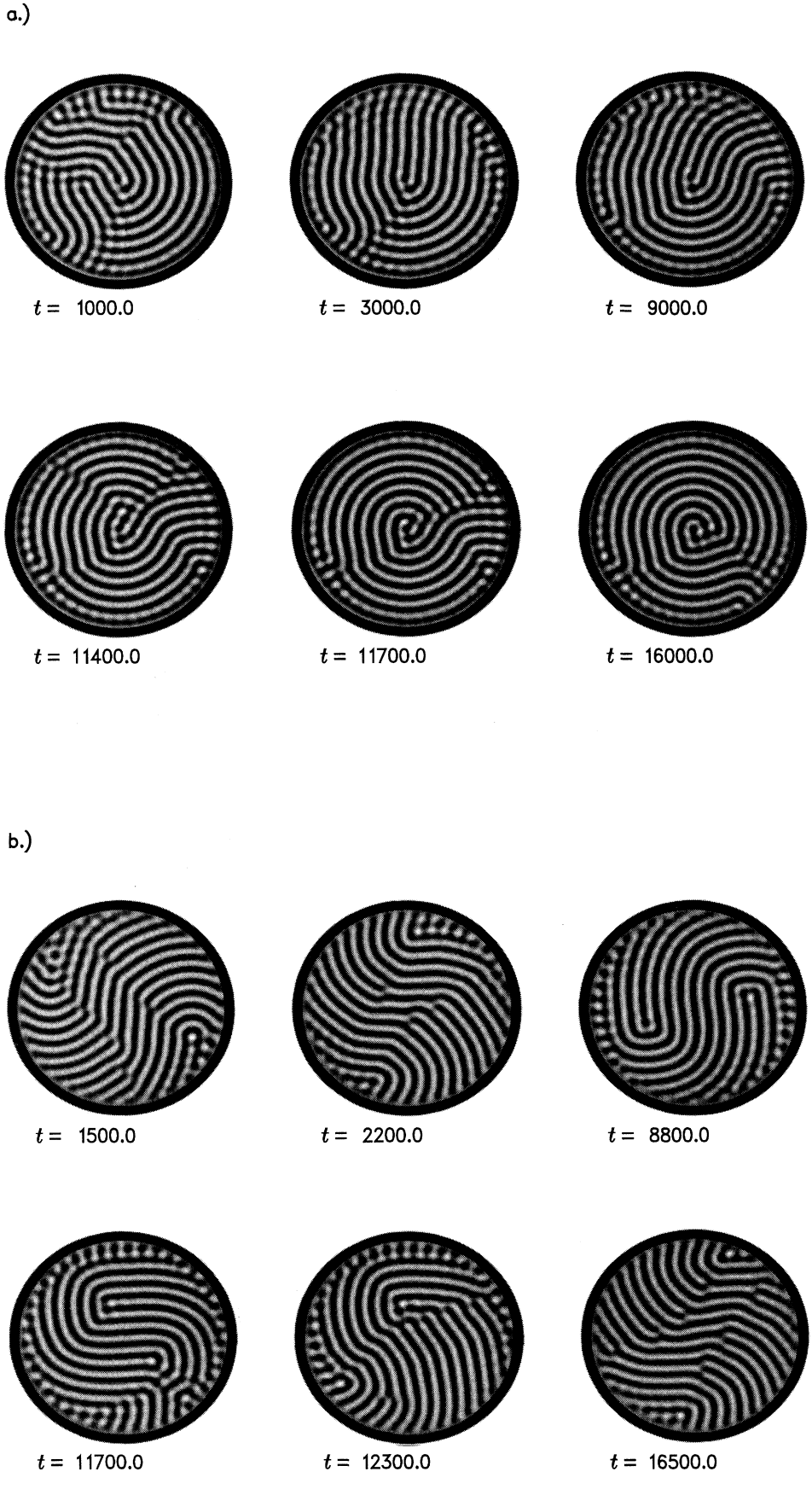

FIG. 4. (a) Sequence of the temporal evolution of the order parameter field in the case of lateral forcing $d=0.1$ and a rotation rate below the critical value for the Küppers-Lortz instability $\mathrm{Ta}_c \approx 2.8$ ($\mathrm{Ta}=1.5$, $\varepsilon=0.1$). (b) Same as (a) but with a Taylor number above the critical one ($\mathrm{Ta}=3.0$, $\varepsilon=0.1$). Here the spiral pattern is formed. However, it is destroyed by the Küppers-Lortz instability but reappears again. In the course of time, a continuous emergence and destruction of the spiral pattern is observed.

We have investigated the dynamics of these patterns by looking at the temporal evolution of the Nusselt number. The time signal of the Nusselt number shows plateaus that are related to different possible excited modes in the periodic vessel. These excited modes are straight convective rolls with different wavelength. The ordered roll pattern lasts for up to some hundred vertical diffusion times, whereas the reorientation is completed after 10–50 verti-

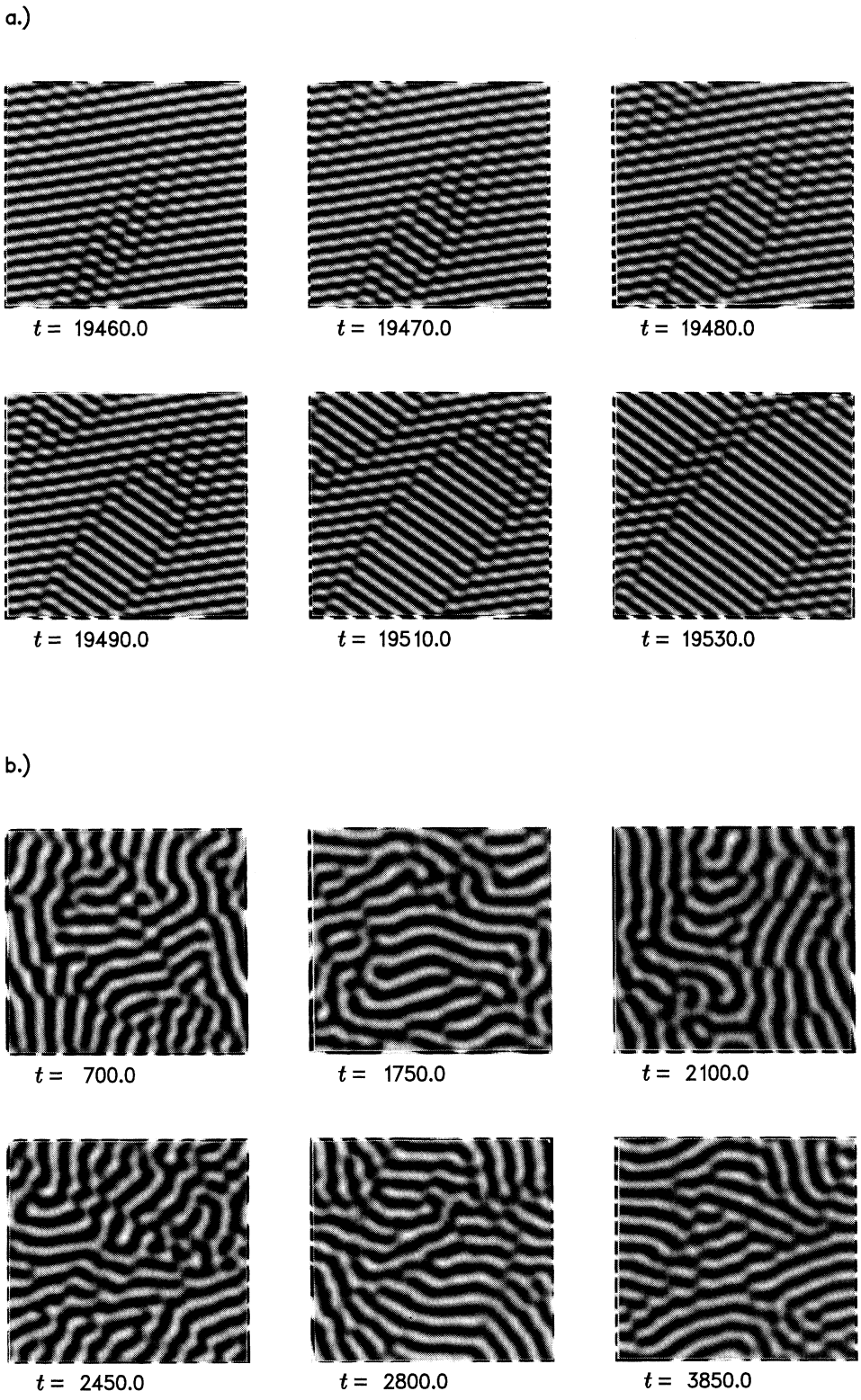

FIG. 5. Patterns in systems with periodic boundary conditions. (a) Küppers-Lortz instability leading to a change in the role direction due to the local nucleation of regions with differently oriented convection rolls. (b) Disordered patterns due to Küppers-Lortz turbulence.

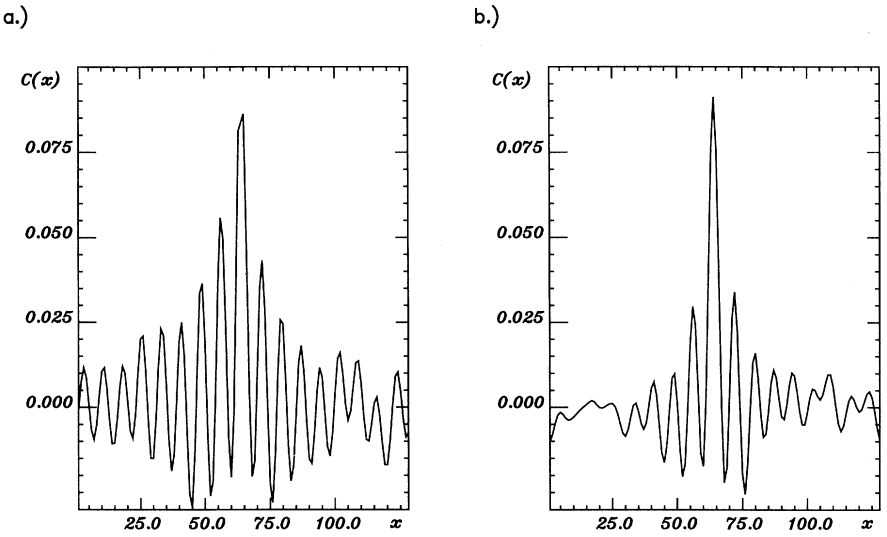

FIG. 6. Spatial correlation functions (11). (a) Ta=7.0. (b) Ta=15.0.

cal diffusion times. This leads to very sharp spikes in the Nusselt number. The time signal is rather intermittent. The time between two successive reorientations is a random quantity.

In order to check whether the different plateaus are related with roll patterns with different wavelength, we have calculated some kind of spatial mean value of the square of the wave vector **k** according to

$$\langle \mathbf{k}^2 \rangle = -\frac{\int d\mathbf{x}\, \psi(\mathbf{x},t)\Delta\psi(\mathbf{x},t)}{\int d\mathbf{x}\, \psi^2(\mathbf{x},t)} . \tag{10}$$

The strong correlation between the jumps in the mean wave number and the spikes in the Nusselt-number signal, related to the Küppers-Lortz change of direction, is evident (see Fig. 8).

Thus the following picture emerges. The model equation in a periodic region allows for various roll solutions differing in wavelength and orientation. All these fixed points are unstable and the system jumps from fixed point to fixed point in the course of time.

For higher Taylor numbers, the patterns break up into small regions consisting of convective rolls of different orientations [see Fig. 5(b)]. Each region shows the reorientation of the roll direction characteristic of the Küppers-Lortz instability. However, the shape of the regions vary by front propagation [see Fig. 5(b)]. By an increase of the Taylor number, the size of the patches of equal roll orientation shrinks. The patterns become rather cellular, exhibiting regions with rectangular or even hexagonal cells. The spatial disorganization of the patterns may be seen in a quantitative fashion by calculating the spatial correlation function

$$C(|\mathbf{x}-\mathbf{x}'|) = \lim_{T\to\infty} \frac{1}{T}\int_0^T dt\, \psi(\mathbf{x},t)\psi(\mathbf{x}',t) . \tag{11}$$

This function exhibits a rapid decay for high Taylor numbers (see Fig. 6). the correlation length decreases with increasing Taylor number.

The transition to these irregular patterns is also evident from the temporal behavior of the Nusselt number. The intermittent behavior ceases to exist. At high Taylor numbers, the Nusselt number fluctuates around a mean value.

V. STATISTICAL PROPERTIES OF THE "NUSSELT NUMBER"

The Nusselt number characterizing the global heat transport across the fluid layer is a quantity of considerable theoretical as well as practical interest. In the case of the disordered patterns arising at high Taylor numbers ($\mathrm{Ta} > 2\ \mathrm{Ta}_c$), it is a fluctuating quantity.

In order to use the following theory, the aspect ratio of the system has to be bigger than the corresponding spatial correlation length to ensure that there are patches of different orientated rolls. Therefore it is tempting to consider its statistical properties.

The Nusselt number is related to the following quantity (8):

$$b = \frac{1}{A}\int d\mathbf{x}\, \psi_s(\mathbf{x},t) = -2\frac{1}{A}\int d\mathbf{x}\, \psi(\mathbf{x},t)\Delta\psi(\mathbf{x},t) . \tag{12}$$

(The second expression can be obtained by a partial integration.) Using the model equation (1), we can derive the following evolution equation:

$$\begin{aligned}\dot{b}(t) &= -\frac{4}{A}\int d\mathbf{x}\, \dot{\psi}(\mathbf{x},t)\Delta\psi(\mathbf{x},t) \\ &= 2\epsilon b(t) + 4\frac{1}{A}\int \Delta\psi(1+\Delta)^2\psi d\mathbf{x} \\ &\quad -4\frac{1}{A}\int \psi_s(\Delta\psi)^2 d\mathbf{x} + 4\frac{1}{A}\int \psi_s \Delta\nabla\psi\cdot\nabla\psi\, d\mathbf{x} \\ &\quad -4\,\mathrm{Ta}\frac{1}{A}\int \Delta\psi \mathbf{e}_3\cdot[\nabla\psi\times\nabla\psi_s]d\mathbf{x} .\end{aligned} \tag{13}$$

Then we can rewrite the integrals as follows:

$$\int \psi_s[(\Delta\psi)^2-\nabla\Delta\psi\cdot\nabla\psi]d\mathbf{x} = \int \psi_s^2 d\mathbf{x}+\int \psi_s[\Delta\psi(\Delta\psi+\psi)-\nabla\psi\cdot\nabla(\Delta\psi+\psi)]d\mathbf{x} , \tag{14}$$

$$\int \Delta\psi \mathbf{e}_3\cdot[\nabla\psi\times\nabla\psi_s]d\mathbf{x}=\int \psi_s\mathbf{e}_3\cdot[\nabla\Delta\psi\times\nabla\psi] . \tag{15}$$

For the following, it is important to remind the reader that for a roll solution (5) the field $\psi_s(\mathbf{x},t)$ is a constant (1). Furthermore, for rolls with wave number close to 1, the quantity $(1+\Delta)\psi$ is small. Since the patterns consist of large portions of rolls, it is therefore possible to perform the approximations

$$\begin{aligned}
&\frac{1}{A}\int \psi_s^2 d\mathbf{x}\approx b^2 ,\\
&\frac{1}{A}\int \psi_s[\Delta\psi(1+\Delta)\psi-\nabla\psi\cdot\nabla(1+\Delta)\psi\, d\mathbf{x}\\
&\qquad\approx b\frac{1}{A}\int [\Delta\psi(1+\Delta)]\psi-\nabla\psi\cdot\nabla(1+\Delta)\psi\, d\mathbf{x}\\
&\qquad=2b\frac{1}{A}\int \Delta\psi(1+\Delta)]\psi\, d\mathbf{x} ,\\
&\frac{1}{A}\int \psi_s\mathbf{e}_3\cdot[\nabla\Delta\psi\times\nabla\psi]d\mathbf{x}\approx b\frac{1}{A}\int \mathbf{e}_3\cdot[\nabla\Delta\psi\times\nabla\psi]d\mathbf{x}=0 .
\end{aligned} \tag{16}$$

We may justify these approximations using the following argument, which is essentially a mean-field-type argument. To this end, we consider the space integral as an average, so that the expressions (16) can be interpreted as higher moments of the field $\psi(\mathbf{x},t)$ and its derivatives. Then the approximations (16) are factorizations of fourth order moments into products of second order moments. From (13) comes the following differential equation for the quantity b:

$$\dot{b}=2\epsilon b-4b^2+bF(t)+f(t) . \tag{17}$$

The time dependent forces $F(t)$ and $f(t)$ are defined as follows:

$$\begin{aligned}
F(t)&=8\frac{1}{A}\int \Delta\psi(\mathbf{x},t)(1+\Delta)\psi(\mathbf{x},t)d\mathbf{x} ,\\
f(t)&=4\frac{1}{A}\int \Delta\psi(\mathbf{x},t)(1+\Delta)^2\psi(\mathbf{x},t)d\mathbf{x} .
\end{aligned} \tag{18}$$

The density of these forces is essentially different from zero in regions where the pattern differs from roll solutions with wave number $k=1$. Therefore, these quantities mark the occurrence of defects, domain walls, and cellular patterns. Furthermore, since they are spatial averages, it is expected on the basis of the central limit theorem that they are quantities with Gaussian statistics in the case of the disordered patterns of Küppers-Lortz turbulence. This can be verified by evaluating the corresponding distribution functions as shown in Fig. 7.

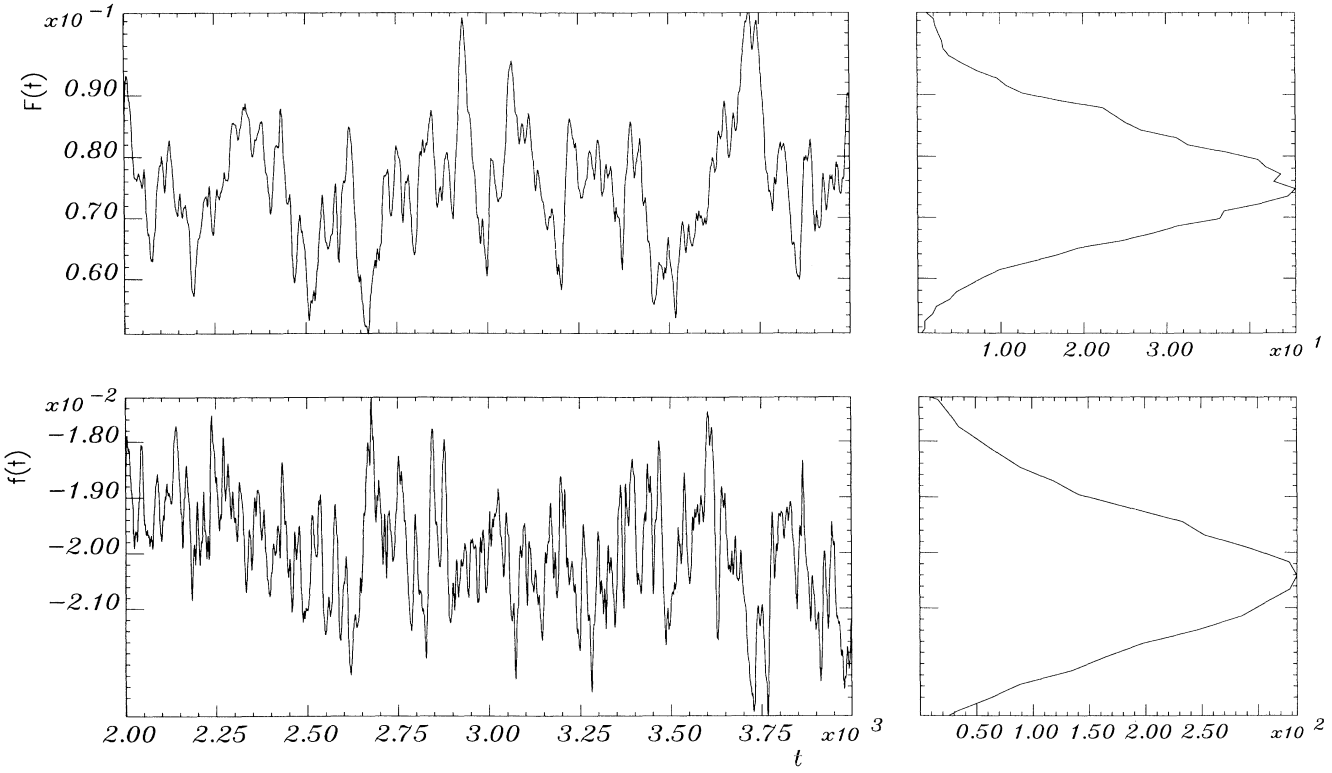

FIG. 7. Time signals of the fluctuating forces [$F(t)$: multiplicative, $f(t)$: additive] versus time for Taylor number Ta=15 and ε=0.1 in a periodic boundary layer. Beside the probability distributions of the fluctuating forces are shown.

In order to check whether our approximations leading to the stochastic equation for the quantity b are justified, we have calculated the time series of $b(t)$ as well as $F(t)$ and $f(t)$ from the numerical treatment of the model equation. Then we can compare the time series of $b(t)$ obtained from the integration of the stochastic equation (17) inserting the calculated time series of $F(t)$ and $f(t)$. Figure 8 shows a comparison of both indicating the accuracy of the above approximations.

Furthermore, the temporal correlations of the patterns decay rapidly and we can consider the white noise limit of Eq. (17). To this end, we assume the force $F(t)-\bar{F}$, as well as $f(t)-\bar{f}$ to be Gaussian white noise (cf. Fig. 7). Both quantities are assumed to have a mean value and to be δ correlated in time,

$$\begin{aligned} &\langle F(t)\rangle=\bar{F}, \quad \langle f(t)\rangle=\bar{f}\ , \\ &\langle [F(T)-\bar{F}][F(t')-\bar{F}]\rangle=Q_{FF}\delta(t-t')\ , \\ &\langle [F(t)-\bar{f}][f(t')-\bar{f}]\rangle=Q_{Ff}\delta(t-t')\ , \\ &\langle [f(t)-\bar{f}][f(t')-\bar{f}]\rangle=Q_{ff}\delta(t-t')\ . \end{aligned} \tag{19}$$

Thus the dynamical system for the quantity b is a stochastic system that has been studied in the context of an instability in the presence of multiplicative and additive noise [15]. The stochastic differential equation then contains the three unknown quantities Q_{FF}, Q_{Ff}, Q_{ff}. How-

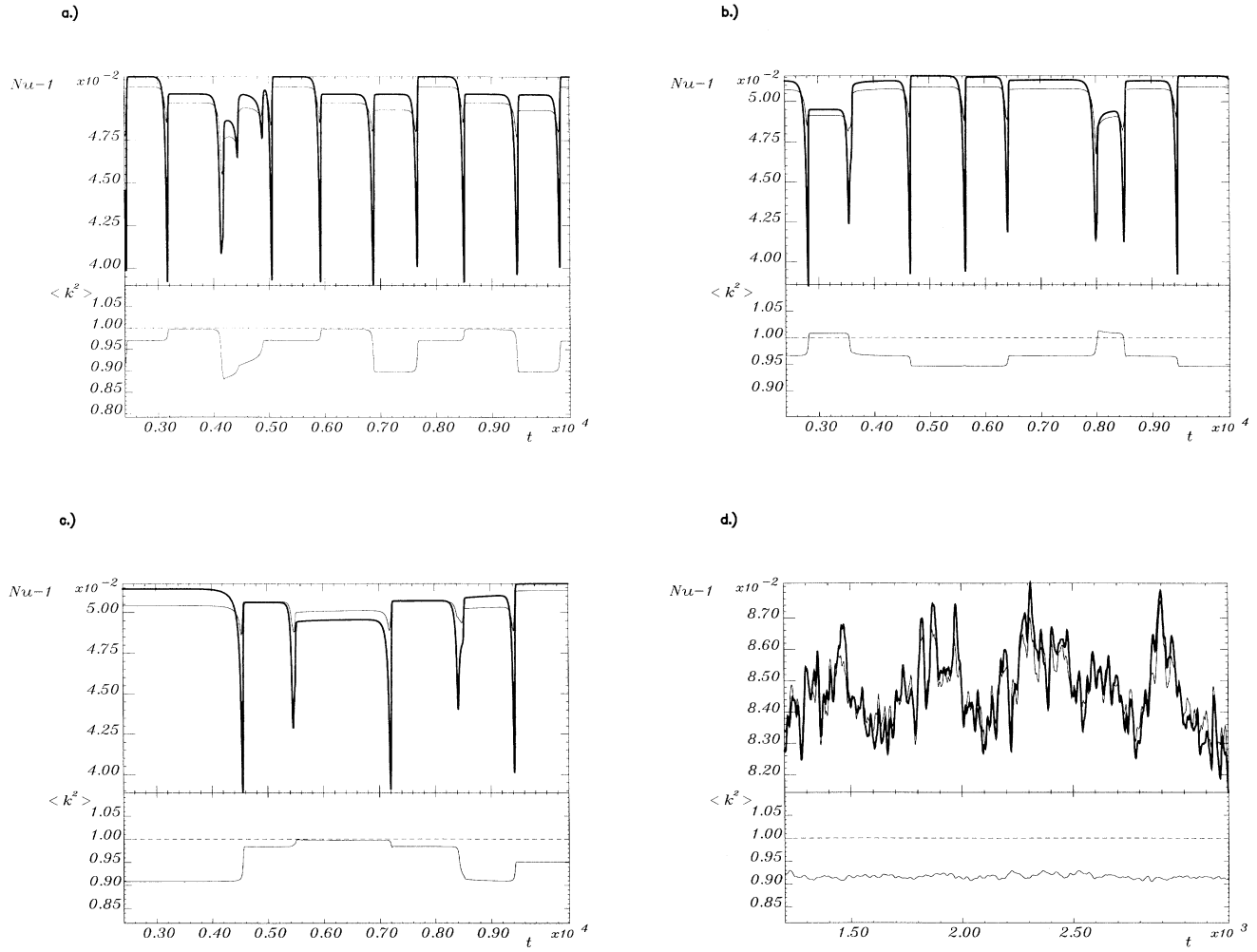

FIG. 8. Time signal of the shifted Nusselt number $\tilde{\mathrm{N}}\mathrm{u}=\mathrm{Nu}-1$ (thick line) compared to the one obtained from the integration of Eq. (17) (thin line). The lower signal shows the mean value $\langle \mathbf{k}^2\rangle$ as defined in Eq. (8). (a) Ta=5.0, $\varepsilon=0.2$, aspect ratio $\Gamma=6$. The spatial correlation length exceeds the periodicity length of the fluid layer. Therefore, one observes a rather coherent behavior. The Nusselt number shows an intermittent temporal behavior. The different plateau values are related to a shift in the average absolute value of the wave vector. The corresponding patterns are roll patterns differing in the wavelength of the rolls. (b) Same as (a) but with aspect ratio $\Gamma=9$. (c) Same as (a) but with aspect ratio $\Gamma=13$. (d) Ta=8.0, $\varepsilon=0.1$, $\Gamma=9$. The Nusselt number fluctuates around a certain mean value.

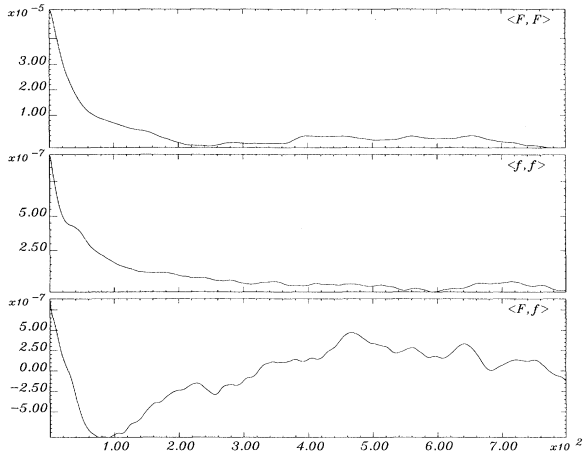

FIG. 9. Temporal auto- and cross-correlation functions of the fluctuating force versus τ ($\langle F(t+\tau)F(t)\rangle$, $\langle f(t+\tau)f(t)\rangle$, and $\langle F(t+\tau)f(t)\rangle$). $F(t)$ is the multiplicative and $f(t)$ the additive noise term.

ever, since we have evaluated the correlation functions (19) from the numerical integration of the model equation, we can determine the noise strength Q_{ff} in the following way (similar expressions hold for Q_{FF}, Q_{Ff})

$$Q_{ff}=2\int_0^\infty dt'\langle[f(t)-\bar{f}][f(t')-\bar{f}]\rangle \ . \tag{20}$$

Since we want to interpret the quantities as Gaussian white noise forces, we can determine the distribution of the quantity b by solving the corresponding Fokker-Planck equation (Fig. 9). Therefore we introduce a deviation $\bar{b}(t)$ from the temporal mean value b_0 that is equivalent with the stationary solution of Eq. (17) with vanishing noise strengths Q_{FF}, Q_{Ff}, $Q_{ff}\to 0$,

$$b_0=\frac{2\epsilon+\bar{F}+\sqrt{(2\epsilon+\bar{F})^2+16\bar{f}}}{8} \ . \tag{21}$$

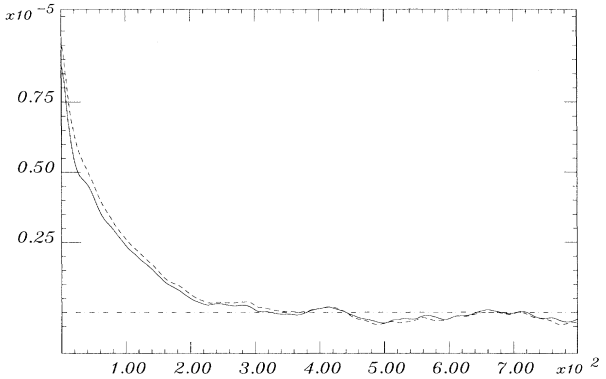

FIG. 10. Comparison of the temporal autocorrelations from the signal of the shifted Nusselt number $\mathrm{Nu}(t)-1$ (solid line)and $b(t)$ [dotted line, from Eq. (17)] for the control parameters $\mathrm{Ta}=15$, $\epsilon=0.1$.

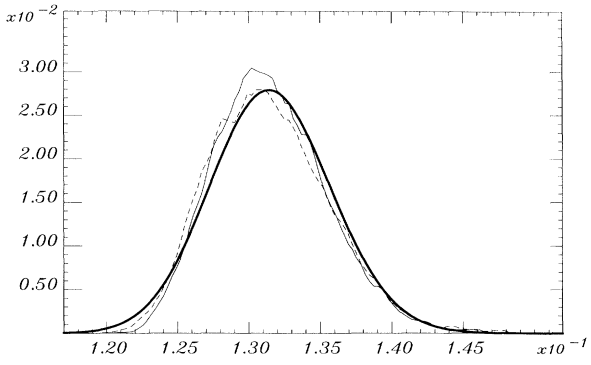

FIG. 11. Histograms of $\mathrm{Nu}-1$ (solid line) and b (dotted line) compared to the probability function (24 bold line) for the noise strength parameters Q_{FF}, Q_{Ff}, and Q_{ff}, which have been calculated from the corresponding correlation functions (cf. Fig. 9).

In an analogous way, we introduce noise forces $\tilde{F}(t)=F(t)-\bar{F}$ and $\tilde{f}(t)=f(t)-\bar{f}$ to obtain from (17) the following stochastic differential equation:

$$\begin{aligned}&\dot{\tilde{b}}(t)=-\gamma\tilde{b}(t)-4\tilde{b}^2(t)+\tilde{b}(t)\tilde{F}(t)+G(t) \ ,\\ &\gamma=\sqrt{(2\epsilon+\bar{F})^2+16\bar{f}} \ ,\\ &G(t)=b_0\tilde{F}(t)+\tilde{f}(t) \ .\end{aligned} \tag{22}$$

In the following we shall skip the tilde. But we have to keep in mind that now all time dependent quantities have a vanishing mean value (Fig. 10).

It is convenient to change from the Langevin equation to the Fokker-Planck description. Using the Stratonovich interpretation, the following Fokker-Planck equation for the distribution function $p(b,t)$ arises:

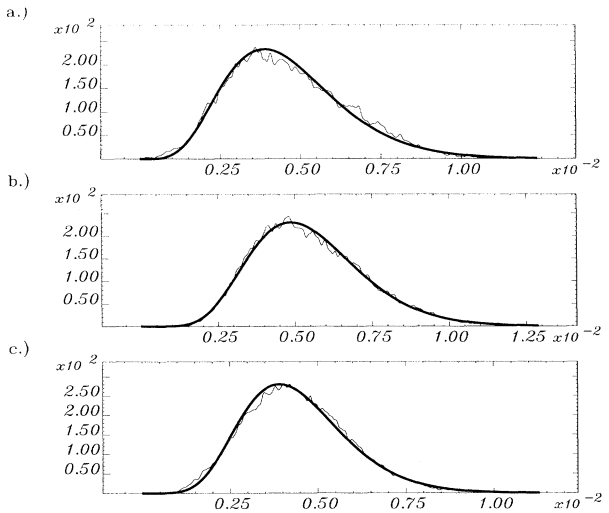

FIG. 12. Histograms of $\mathrm{Nu}-1$ (thin line) compared to the probability function (30) for different Taylor numbers. (a) $\mathrm{Ta}=13$, (b) $\mathrm{Ta}=14$, (c) $\mathrm{Ta}=15$.

$$\dot{p}(b,t)=-\frac{\partial}{\partial b}[-\gamma b-4b^2+\tfrac{1}{2}Q_{FF}b+\tfrac{1}{2}Q_{FG}]p(b,t)+\frac{Q_{FF}}{2}\frac{\partial^2}{\partial b^2}b^2p(b,t)+Q_{FG}\frac{\partial^2}{\partial b^2}bp(b,t)+\frac{Q_{GG}}{2}\frac{\partial^2}{\partial b^2}p(b,t)\ . \tag{23}$$

The stationary solution of the Fokker-Planck equation can be calculated in a straightforward manner by performing the following integral:

$$\ln[p(b)]=\int_{-\infty}^{b}db'\frac{-8b'^2-(2\gamma+Q_{FF})b'-Q_{FG}}{Q_{FF}b'^2+2Q_{FG}b'+Q_{GG}}\ , \tag{24}$$

where

$$\begin{aligned}&\langle G,F\rangle=\langle b_0F+f,F\rangle=b_0\langle F,F\rangle+\langle f,F\rangle\ ,\\&\langle G,G\rangle=\langle b_0F+f,b_0F+f\rangle\\&\quad=b_0^2\langle F,F\rangle+2b_0\langle f,F\rangle+\langle f,f\rangle\ ,\\&Q_{FG}=b_0Q_{FF}+Q_{Ff}\ ,\\&Q_{GG}=b_0^2Q_{FF}+2b_0Q_{Ff}+Q_{ff}\ .\end{aligned} \tag{25}$$

The integral (24) can be integrated analytically. Its main contribution is an exponential function $\exp(-8/Q_{FF}b)$ times a polynomial in b. Figure 11 shows the distribution function $p(b)$ calculated from the Fokker-Planck equation and the distribution function $p(b)$ as obtained from the direct numerical evaluation of our model equation (1).

If we consider the case of large Taylor numbers $\mathrm{Ta}>3\,\mathrm{Ta}_c$, it turns out that the quantities Q_{Ff}, Q_{ff} as well as $\bar{f}$ become much smaller as compared to Q_{FF}. Therefore, we obtain the following Fokker-Planck equation:

$$\dot{p}(b,t)=-\frac{\partial}{\partial b}[(2\epsilon+\bar{F})b-4b^2+\tfrac{1}{2}Q_{FF}b]p(b,t)+\frac{Q_{FF}}{2}\frac{\partial^2}{\partial b^2}b^2p(b,t)\ . \tag{26}$$

Then the corresponding stationary distribution function is given by

$$p(b)=N\exp\left[-\frac{8}{Q_{FF}}b\right]b^{[(4\epsilon+2\bar{F}/Q_{FF})-1]}\ . \tag{27}$$

The moments $\langle b^n\rangle$ can be easily calculated:

$$\langle b^n\rangle=\left\{\frac{Q_{FF}}{8}\right\}^n\frac{\Gamma\left[\frac{4\epsilon+2\bar{F}}{Q_{FF}}+n\right]}{\Gamma\left[\frac{4\epsilon+2\bar{F}}{Q_{FF}}\right]}=\left\{\frac{Q_{FF}}{8}\right\}^n\prod_{i=1}^{n}\left[\frac{4\epsilon+2\bar{F}}{Q_{FF}}+i-1\right]$$

$$=\langle b^{n-1}\rangle\frac{Q_{FF}}{8}\left[\frac{4\epsilon+2\bar{F}}{Q_{FF}}+n-1\right]\ . \tag{28}$$

Since the distribution function depends on two parameters $\tilde{\epsilon}=\epsilon+\frac{1}{2}\bar{F}$, Q_{FF}, the knowledge of two of these moments determines the distribution function uniquely:

$$4\epsilon+2\bar{F}=8\langle b\rangle,\quad Q_{FF}=8\frac{\langle b^2\rangle-\langle b\rangle^2}{\langle b\rangle}\ . \tag{29}$$

Therefore, an experimentalist could calculate the first two moments $\langle b\rangle$ and $\langle b^2\rangle$ of the time series of b; the distribution function should be fitted very well by

$$p(b)=N\exp\left[-\frac{\langle b\rangle b}{\langle b^2\rangle-\langle b\rangle^2}\right]b^{[\langle b\rangle^2/(\langle b^2\rangle-\langle b\rangle^2)-1]}\ . \tag{30}$$

Figure 12 shows a comparison of the distribution function of the Nusselt number and (30) in the numerical experiment with increasing Taylor number; the distribution approaches a Gaussian for increasing Taylor number (cf. Fig. 11). In the limiting case $\tilde{\epsilon}/Q_{FF}\to\infty$, the distribution function approaches a Gaussian:

$$\begin{aligned}&f(b)=N\exp\left[-\frac{1}{\sigma^2}(b-b_0)^2\right]\ ,\\&b_0=\frac{\tilde{\epsilon}}{2}-\frac{Q_{FF}}{4\tilde{\epsilon}}\ ,\\&\sigma=\frac{1}{3}\left[\frac{2\tilde{\epsilon}}{Q_{FF}}\right]^{-2}\left[\frac{4}{Q_{FF}}-\frac{1}{2}\right]\ .\end{aligned} \tag{31}$$

Then the quantity b obeys Gaussian statistics as it should be due to the central limit theorem. The Nusselt number is essentially a sum over statistically independent contributions of the quantity $\psi_s(\mathbf{x},t)$ if the spatial correlations of the field $\psi(\mathbf{x},t)$ decay rapidly.

Summarizing, we have shown for our model equation that the global heat transport, i.e., the Nusselt number, in the case of disordered patterns arising due to a Küppers-Lortz type instability, can be described by a stochastic dynamical system, and we were able to determine the stationary probability distribution.

ACKNOWLEDGMENT

One of us (M.N.) is supported by the Deutsche Forschungsgemeinschaft (DFG) under Grant No. DFG FR 1003/1-1.

[1] G. Küppers and D. Lortz, J. Fluid Mech. **35**, 609 (1969).
[2] F. H. Busse and K. E. Heikes, Science **208**, 173 (1980).
[3] Y. Tu and M. C. Cross, Phys. Rev. Lett. **69**, 2515 (1992).
[4] J. Swift and P. C. Hohenberg, Phys. Rev. A **15**, 319 (1977).
[5] M. Neufeld, R. Friedrich, and H. Haken, Z. Phys. B **92**, 243 (1993).
[6] H. Haken, *Synergetics. An Introduction,* 3rd ed. (Springer-Verlag, Berlin, 1983).
[7] H. Haken, *Advanced Synergetics,* 2nd ed. (Springer-Verlag, Berlin, 1987).
[8] M. Frantz, R. Friedrich, M. Bestehorn, and H. Haken, *Evolution of Patterns in Rotating Bénard Convection, in em From Phase Transition to Chaos* (World Scientific, Singapore, 1992), pp. 118–127.
[9] M. Fantz, R. Friedrich, M. Bestehorn, and H. Haken, Physica D **61**, 147 (1992).
[10] R. M. Clever and F. H. Busse, J. Fluid Mech. **94**, 609 (1979).
[11] F. Zhong and R. Ecke, Chaos **2**, 163 (1992).
[12] J. K. Platten and J. C. Legros, *Convection in Liquids* (Springer, Berlin, 1984).
[13] F. Zhong, R. Ecke, and V. Steinberg, Physica D **51**, 596 (1991).
[14] F. H. Busse, in *Chaos and Order in Nature,* edited by H. Haken (Springer-Verlag, Berlin, 1981).
[15] W. Horsthemke and R. Lefever, *Noise-Induced Transitions,* Springer Series Synergetics Vol. 15 (Springer, Berlin, 1983).

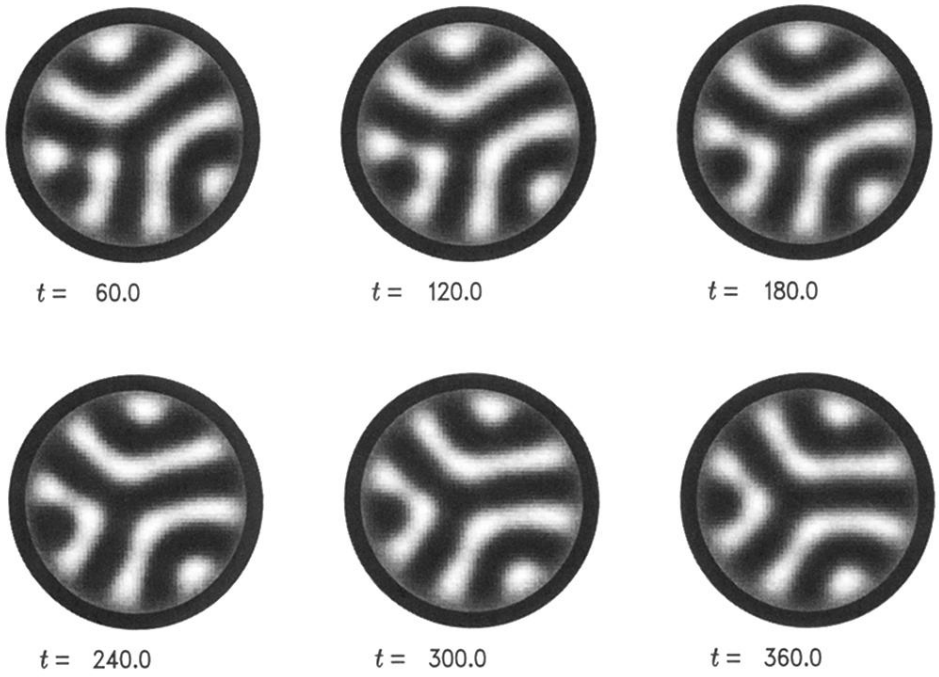

FIG. 2. Temporal evolution of convection patterns in a low aspect ratio system for a small rotation rate. The pattern is formed by three foci that are located at the lateral boundary. The pattern is drifting very slowly.

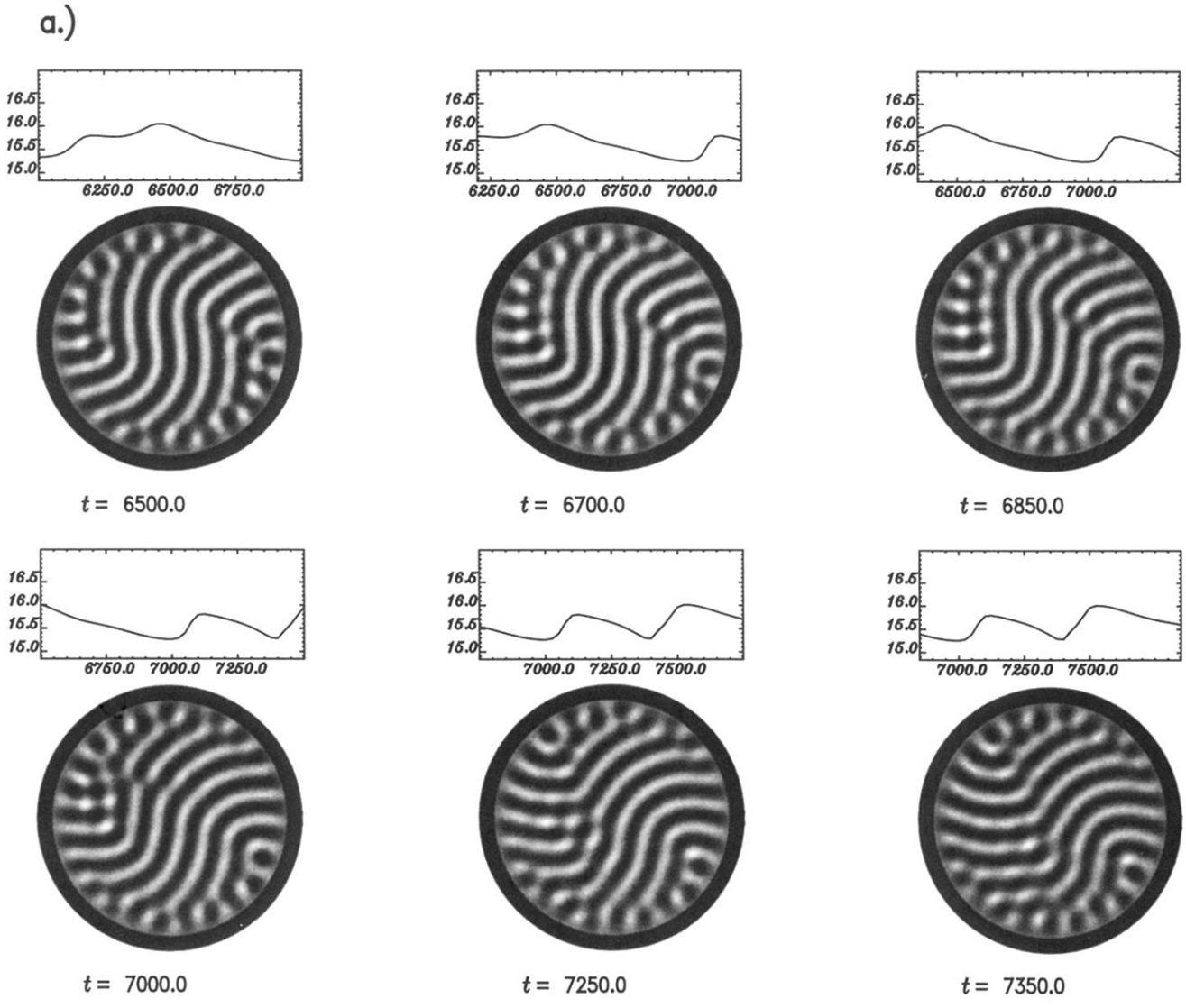

FIG. 3. Temporal evolution of the order parameter field and the Nusselt number in the case of vanishing lateral forcing $d=0.0$ and $\varepsilon=0.1$. (a) Defect motion in the case of a Taylor number $\mathrm{Ta}=2.0<\mathrm{Ta}_c$. (b) Front propagation in the case of a Taylor number $\mathrm{Ta}=3.0>\mathrm{Ta}_c$.

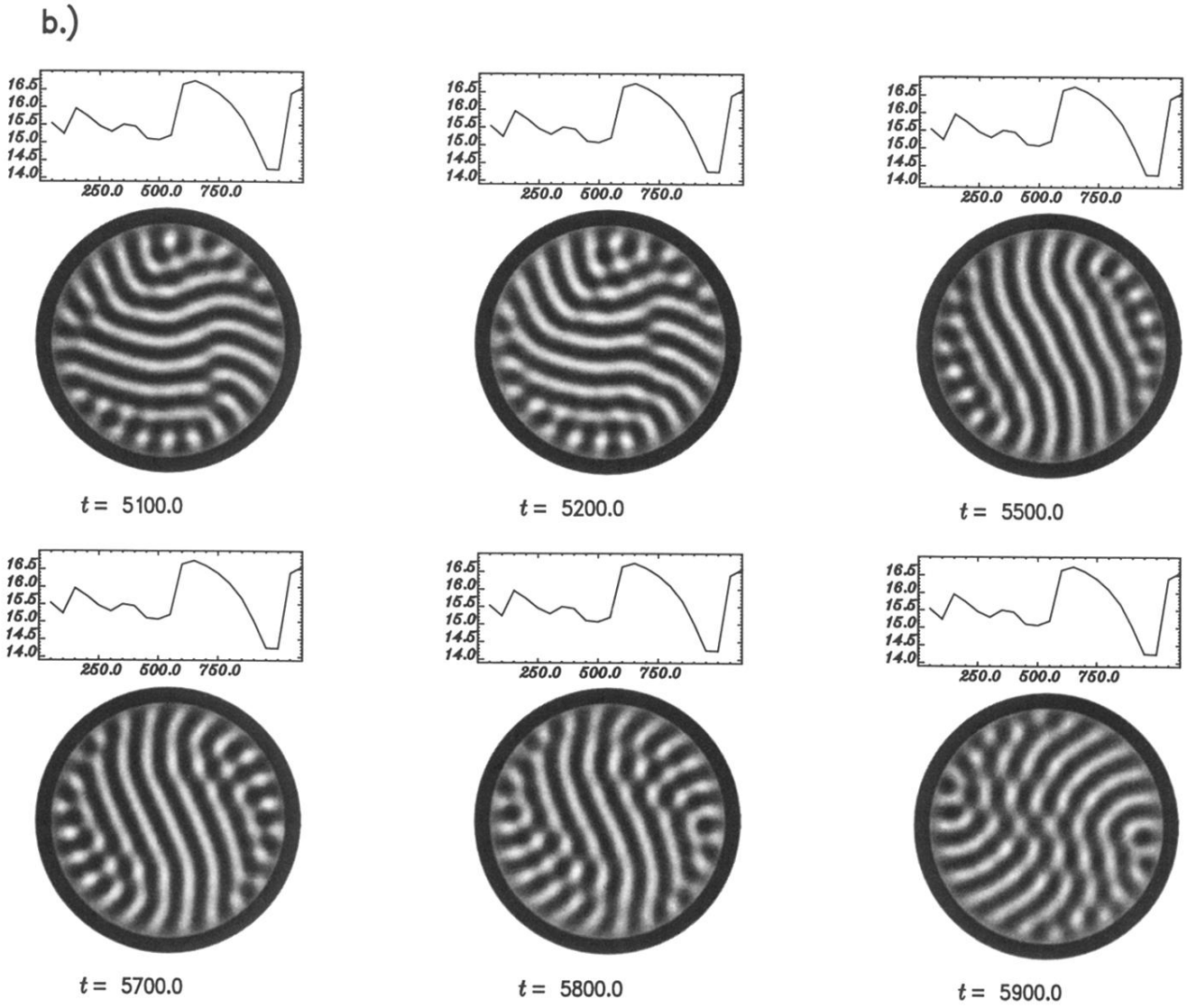

FIG. 3. (*Continued*).

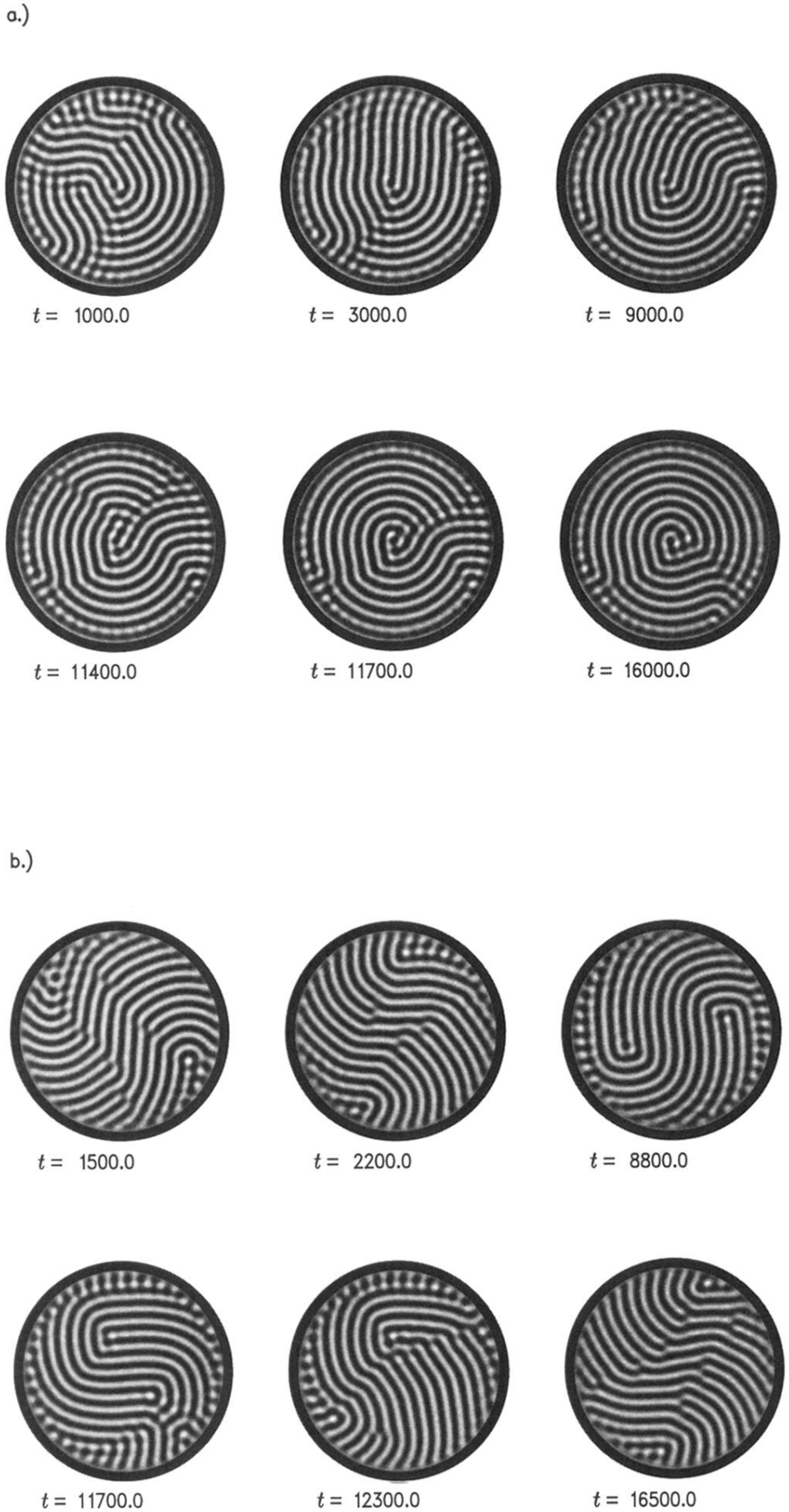

FIG. 4. (a) Sequence of the temporal evolution of the order parameter field in the case of lateral forcing $d=0.1$ and a rotation rate below the critical value for the Küppers-Lortz instability $\mathrm{Ta}_c \approx 2.8$ ($\mathrm{Ta}=1.5$, $\varepsilon=0.1$). (b) Same as (a) but with a Taylor number above the critical one ($\mathrm{Ta}=3.0$, $\varepsilon=0.1$). Here the spiral pattern is formed. However, it is destroyed by the Küppers-Lortz instability but reappears again. In the course of time, a continuous emergence and destruction of the spiral pattern is observed.

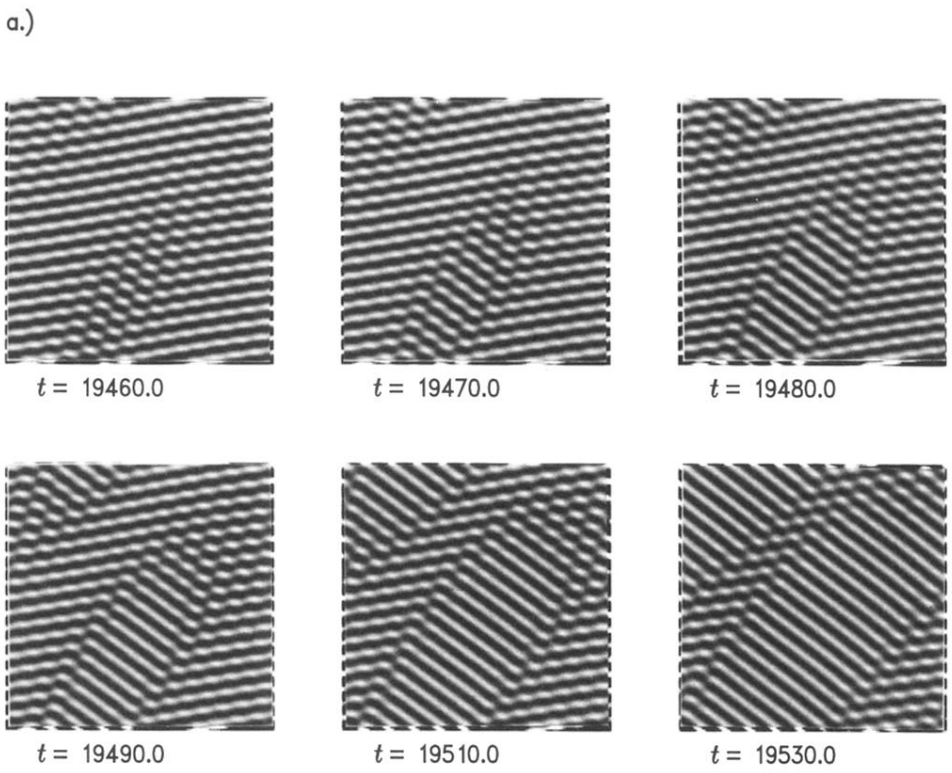

FIG. 5. Patterns in systems with periodic boundary conditions. (a) Küppers-Lortz instability leading to a change in the role direction due to the local nucleation of regions with differently oriented convection rolls. (b) Disordered patterns due to Küppers-Lortz turbulence.